ENVIRONMENTAL ENGINEERING SCIENCE
Volume 00, Number 00, 2017

DOI: 10.1089/ees.2016.0540

ORIGINAL ARTICLE

Statistical Model and Estimation of Inland Riverine Turbidity with Landsat 8 OLI Images: A Case Study

Xin Shen[1–3] and Qi Feng[4,5,*]

[1]State Key Laboratory of Information Engineering in Surveying, Mapping and Remote Sensing, Wuhan University, Wuhan, China.
[2]Collaborative Innovation Center of Geospatial Technology, Wuhan, China.
[3]School of Resources and Environmental Sciences, Wuhan University, Wuhan, China.
[4]Institute of Geodesy and Geophysics, Chinese Academy of Sciences, Wuhan, China.
[5]Key Laboratory for Environment and Disaster Monitoring and Evaluation, Hubei, China.

Received: October 27, 2016 *Accepted in revised form: May 25, 2017*

Abstract

The Landsat 8 Operational Land Imager (OLI) was investigated for its performance in monitoring dynamic riverine surface water turbidity. China's Hanjiang River, the largest tributary of the Yangtze River, was used as a case study. Field surveys conducted between April 2013 and January 2014 show a wide range of turbidity (15.8–130.2 nephelometric turbidity units). A practical exponential retrieval algorithm used in conjunction with OLI bands on Landsat 8 was developed to assess compatibility between satellite remote sensing reflectance and *in situ* measured data. Results obtained for the study area accurately match *in situ* data at most stations ($R^2 > 0.90$) for the validation phase. It was found that Landsat 8 OLI imagery can be used to estimate turbidity in inland riverine systems when a suitable retrieval algorithm is applied. In addition, algal blooms in the riverine system can be detected by OLI imagery.

Keywords: algae bloom; Landsat 8; Hanjiang River; riverine systems; turbidity

Introduction

Turbidity (Tur) is considered a key water quality variable due to its impact on light suppression, biochemical oxygen demand, sediment-associated contaminant transport, and suspended sediment loads, which affect organisms and inland riverine habitats (Lawler *et al.*, 2006; Davies-Colley *et al.*, 2011; Jones *et al.*, 2012). Owing to unique optical properties of turbidity, this parameter can be estimated from remotely sensed data, thus achieving wide spatial and temporal coverage compared with traditional sampling methods (Simis *et al.*, 2007; Guttler *et al.*, 2013).

Well-established algorithms for recurrent ocean sensor monitoring of turbidity exist, employing reflectance in the blue and green color regions of oceans (Gordon and Franz, 2008; Neukermans *et al.*, 2012). However, these algorithms may not be appropriate for inland water systems such as rivers due to differing optical properties of sea water bodies (Le *et al.*, 2011; Yacobi *et al.*, 2011; Li *et al.*, 2012). Although some ocean color sensors possess short revisit times with high spectral resolution and sensitivity, which makes them suitable for studies of some inland water bodies such as large lakes or reservoirs (Shi *et al.*, 2014, 2015; Zhang *et al.*, 2016a), their spatial resolution is typically too coarse to adequately investigate riverine features, making them unsuitable for monitoring water quality variations in these systems (Ghabavati *et al.*, 2008; Onderka and Pekárová, 2008; Yu *et al.*, 2012).

Landsat sensors, such as the Landsat 5 (Thematic Mapper) and Landsat 7 (Enhanced Thematic Mapper Plus), may have longer revisit times and lower spectral and radiometric resolution than ocean-specific instruments, but possess higher spatial resolution. Accordingly, those sensors have been used for inland water studies (Vincent *et al.*, 2004; Ma *et al.*, Onderka and Pekárová, 2008; Kuster, 2012).

After the retirement of Landsat 5, the failure of Landsat 6, and limitations with Landsat 7, the Landsat 8 satellite was launched on February 11, 2013, and operations began on May 30 of the same year. With its nine bands, Landsat 8 imagery provides sufficient spatial resolution, in which features such as islands within rivers and bridges spanning rivers can be easily distinguished as highly reflective structures before a dark background (Vanhellemont and Ruddick, 2014). Compared with previous Landsat missions, Landsat 8 also offers higher signal-to-noise ratios. This is primarily the result of

*Corresponding author: Key Laboratory for Environment and Disaster Monitoring and Evaluation, Hubei, China. *Phone:* +86-027-6888-1075; *Fax:* +86-027-6888-1362; *E-mail:* fengqi@asch.whigg.ac.cn

longer integration times associated with the push broom scanner as well as improved quantization (NASA, 2016; USGS, 2016). Because of inclusion of the Operational Land Imager (OLI), Landsat 8 has the potential to become the first Landsat sensor with the radiometric resolution necessary for retrieval of chlorophyll and suspended material constituents in oceans and lakes (Gerace *et al.*, 2013; Pahlevan and Schott, 2013; Wu *et al.*, 2015; Zhang *et al.*, 2016b). However, few studies have applied Landsat 8 images to retrieve riverine water quality parameters.

Rapid economic development and anthropogenic activity in and around Hanjiang River have increased ecological pressure on its water quality, which is of great environmental importance to Hubei Province (Liu and Yu, 1992; Wang *et al.*, 2004; Guo *et al.*, 2014). In addition, the Danjiangkou Dam, which is on the upstream of the Hanjiang River and was originally constructed in 1958, has since been raised, and the Danjiangkou Reservoir, created by the construction of Danjiangkou Dam, has been used as part of the South-to-North Water Diversion Project (SNWDP) since 2014. Research has shown the probability that algal blooms will increase in the mid-downstream region of the Hanjiang River after completion of the SNWDP (Xie *et al.*, 2004).

Therefore, comprehensive monitoring is needed to address changes in water quality in this area. Accordingly, the objectives of this study are to apply and evaluate the use of readily available imagery from Landsat 8 together with published literature to assess water turbidity changes in the inland riverine system.

Study Area and Data Processing

Study area

The Hanjiang River (historically called the Hanshui River) is a major tributary of the Yangtze River and has a total length of 1,577 km. The river originates in the mountainous region of southwestern Shaanxi and flows eastward across the southern expanse of the province. The Qin Mountains are north of the mouth of the river. Further north is the Wei River, the largest tributary of the Yellow River, which forms the southern boundary of the Ordos Loop. The Daba Mountains to the south of the river act as a natural boundary that separates Shaanxi Province from Sichuan Province and Chongqing City. The river flows southeastward through Hubei Province, connecting with the Yangtze River at Wuhan, the provincial capital.

In the study area (Fig. 1), the main cities along the Hanjiang River are Qianjiang City (population 1.1 million) to the west and Xiantao City (population 1.2 million) to the east. Both cities are located in the mid-downstream region of Hanjiang River. The area belongs to the subtropical monsoon climate zone, with mild climate characterized by four distinct

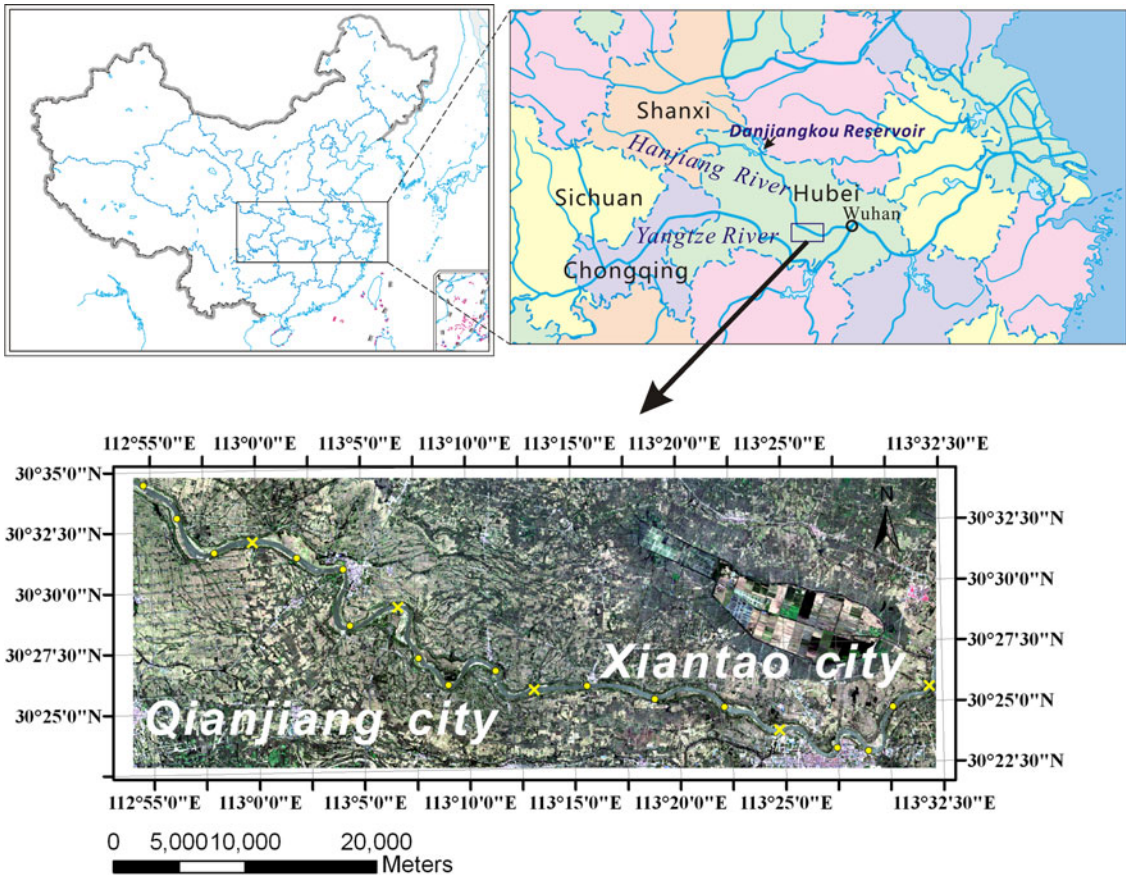

FIG. 1. Mosaic map made with Landsat 8 image (*Red*: 630–680 nm, *Green*: 525–600 nm, *Blue*: 450–515 nm) collected on June 13, 2013, showing the study area and location of Hanjiang River in China. *Yellow points* represent the data of 15 samples for modeling of each image. *Yellow cross* represents the data of 5 samples for validation of each image.

TABLE 1. DESCRIPTION OF *IN SITU* TURBIDITY WITHIN STUDY AREA

Sampling date	*Sampling number*	*Sampling time*	*Turbidity range (NTU)*	*Mean value (NTU)*	*Standard deviation (NTU)*
April 26, 2013	20	02:46UTC–05:39UTC	20.8–49.7	32.3	7.10
June 13, 2013	20	01:52UTC–05:06UTC	39.3–54.4	47.5	4.66
November 20, 2013	20	02:44UTC–06:04UTC	15.8–25.9	20.3	2.62
January 23, 2014	20	01:45UTC–04:56UTC	47.2–130.2	75.5	29.15

NTU, nephelometric turbidity units.

seasons, abundant rainfall, a long (256 days) frost-free period, 2002.6 annual average sunshine hours, and an average annual temperature of 16.3°C. The division into seasons is based on an average temperature below 10°C during winter, a temperature above 22°C during summer, and temperatures between 10°C and 22°C during spring and autumn. Spring lasts from roughly mid-March to mid-May (about 70 days), summer from late May to mid-September (about 120 days), autumn from late September to mid-November (about 65 days), and winter from late November to early March (about 110 days). In the study area, the southern part of the Hanjiang River is characterized by industrial installations, including auto part, pharmaceutical, chemical, electronic, and nonwoven fabric factories, while the northern part of the river is mainly characterized by aquaculture and farming.

Field survey data

Four field surveys were conducted in the study area between April 2013 and January 2014. Twenty water samples were collected during each survey, including 15 samples for modeling and 5 samples for validation (the position of each sample is provided in Fig. 1). In total, 80 water samples for surface turbidity were collected. At each station, the distance between two adjacent data collection sites was 2–3 km. Surface water turbidity was measured *in situ* using a 2100P Hach Turbidimeter (Hach Company, Loveland, Colorado), and the longitudes and latitudes for each sampling location were obtained using a Global Positioning System receiver (Garmin Ltd., Lenexa, KS). Description of measured turbidity is provided in Table 1 and Fig. 2.

Remote sensing data

The OLI instrument on Landsat 8 is a nine-band push broom scanner with a swath width of 185 km, eight channels at 30-m spatial resolution, and one panchromatic channel at 15-m spatial resolution. Five good-quality Level 1T OLI images were obtained from the U.S. Geological Survey (USGS) website (http://earthexplorer.usgs gov). The images covering the area downstream of the Hanjiang River were examined in detail (Table 2). With reference to some published literatures (Shi *et al.*, 2015; Zhang *et al.*, 2016b), turbidity was investigated using OLI band 1 (433–453 nm, which was not featured on previous Landsat satellites), band 2 (450–515 nm), band 3 (525–600 nm), band 4 (630–680 nm), and band 5 (845–885 nm).

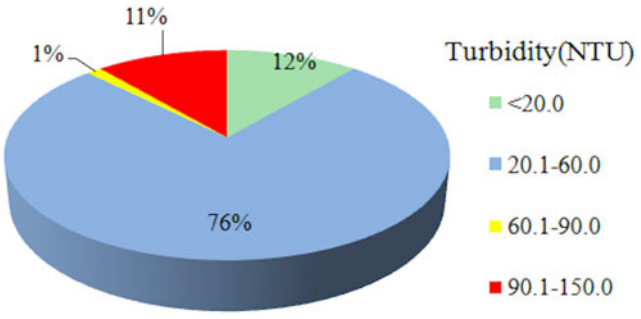

FIG. 2. Distribution of measured turbidity in this study (Total data of 80 samples).

Data preprocessing of OLI imagery

Standard Landsat 8 OLI images consist of quantized, calibrated, and scaled digital numbers (DNs) representing multispectral image data, which are delivered in 16-bit unsigned integer format. The DN values were rescaled to the top-of-atmosphere (TOA) reflectance using the equation provided by the USGS (http://landsat.usgs.gov Landsat8_Using_Product.php).

The TOA reflectance is a linear sum of various contributions, including molecules (Rayleigh scattering), aerosols (Rayleigh–aerosol interactions), and water (Wang *et al.*, 2007). An atmospheric correction is used to derive water-leaving reflectance by removing atmosphere and water surface effects from TOA reflectance. Shortwave infrared (SWIR) bands have much stronger water absorption than near-infrared bands, thus the black water assumption for atmospheric correction is generally valid in the SWIR region, even for very turbid waters (Wang *et al.*, 2007). Therefore, assuming the water-leaving reflectance at the SWIR bands is zero, a simplified method was employed to estimate the water-leaving reflectance of Landsat 8 OLI visible and infrared bands by removing the total atmosphere and water surface effects using Equation (1):

TABLE 2. LANDSAT 8/OLI IMAGES USED

Image	*Date*	*Time*
LC81230392013116LGN01	April 26, 2013	02:58:03UTC
LC81230392013164LGN00	June 13, 2013	02:58:17UTC
LC81230392013324LGN00	November 20, 2013	02:57:56UTC
LC81230392014023LGN00	January 23, 2014	02:57:26UTC
LC81230392015090LGN00	March 1, 2016	02:55:44UTC

OLI, Operational Land Imager.

Table 3. Retrieval Models for Turbidity (Tur) Based on Landsat 8 OLI Bands Obtained During the Establishment Phase

Number	*Formulation*	*X*	R^2	*RMSE*
1	$Tur = 4636.8X^2 - 8104.5X + 3573.8$	Rrs(2)/Rrs(1)	0.52	16.92
2	$Tur = 45.62\times^2 + 11.90X - 31.17$	Rrs(3)/Rrs(1)	0.91	7.21
3	$Tur = 1.16e^{2.80X}$	Rrs(3)/Rrs(2)	0.87	7.93
4	$Tur = 2.57\ e^{2.71X}$	Rrs(4)/Rrs(1)	0.84	9.60
5	$Tur = 1.48\ e^{2.99X}$	Rrs(4)/Rrs(2)	0.85	9.26
6	$Tur = 26.96X^{-0.64}$	Rrs(5)/Rrs(2)	0.24	23.10
7	$Tur = -32.98In(X) + 17.96$	Rrs(5)/Rrs(3)	0.37	19.39
8	$Tur = 24.46X^{-0.71}$	Rrs(5)/Rrs(4)	0.44	21.07
9	$Tur = 1.92\ e^{1.44X}$	Rrs(4)/Rrs(1) + Rrs(4)/Rrs(2)	0.86	9.13
10	$Tur = 4.01 - 28.70X + 18.51X^2$	Rrs(3)/Rrs(2) + Rrs(3)/Rrs(1)	0.92	6.81

R^2, coefficient of determination used for retrieval and measured values obtained from the established database; RMSE, root mean square error.

$$R_{rs}(\lambda) = P_\lambda - P_{SWIR}, \quad (1)$$

where $R_{rs}(\lambda)$ is the water-leaving reflectance at the visible and infrared bands, P_λ is the TOA reflectance with a correction for solar angle at wavelength λ, and P_{SWIR} is the TOA reflectance at the SWIR bands of Landsat 8.

Topographic maps at a scale of 1:50,000 were used to register the atmospherically corrected image to Beijing 54/Gauss–Kruger projection using first-order polynomial and nearest-neighbor resampling methods, and the root mean square error (RMSE) of positional accuracy was within half a pixel. The projected image was reprojected to WGS 84/UTM, and land areas and small water bodies were removed using a binary mask created from unsupervised classification of images.

Formulation of retrieval algorithm

Landsat 8 OLI band satellite $R_{rs}(\lambda)$ data were extracted for sampling after atmospheric correction was performed. Three-quarters (60) of the turbidity data from the first four images were used to calibrate the retrieval model, while the remaining quarter (20) was used for validation.

Several studies have shown that single bands or band combinations from Landsat series imagery can be used in turbidity or suspended matter mapping for inland water systems (Onderka and Pekárová, 2008; Wu *et al.*, 2015). To obtain the optimal retrieval algorithm, descriptive statistics of turbidity measurements and their corresponding Landsat 8 OLI image band 1–5 values were analyzed with the support of SPSS software (IBM. Co., Armonk) to formulate settings. The coefficient of determination (R^2) and RMSE of all calibrated models were compared with select ten regression models with sufficient goodness of fit for estimating turbidity (Table 3).

For each calibrated Landsat 8-based turbidity retrieval model, the coefficient of determination (R^2) between the validation data and estimated turbidity, as well as the RMSE, mean absolute error (MAE), and mean absolute percentage error (MAPE), was calculated to assess the performance of the best, stable, Landsat 8-based turbidity model.

Table 4. Static Index Applied to Models to Validate Turbidity

Number	R^2	*MAE*	*RMSE*	*MAPE (%)*
1	0.54	15.69	19.65	46.58
2	0.89	6.68	7.58	20.06
3	0.87	7.80	9.96	21.05
4	0.86	7.45	9.28	22.12
5	0.84	8.70	11.37	22.35
6	0.35	17.02	24.51	44.06
7	0.56	15.54	19.91	42.88
8	0.61	14.71	20.22	36.92
9	0.88	7.57	9.64	21.51
10	0.93	6.03	7.36	18.96

MAE, mean absolute error; MAPE, mean absolute percentage error.

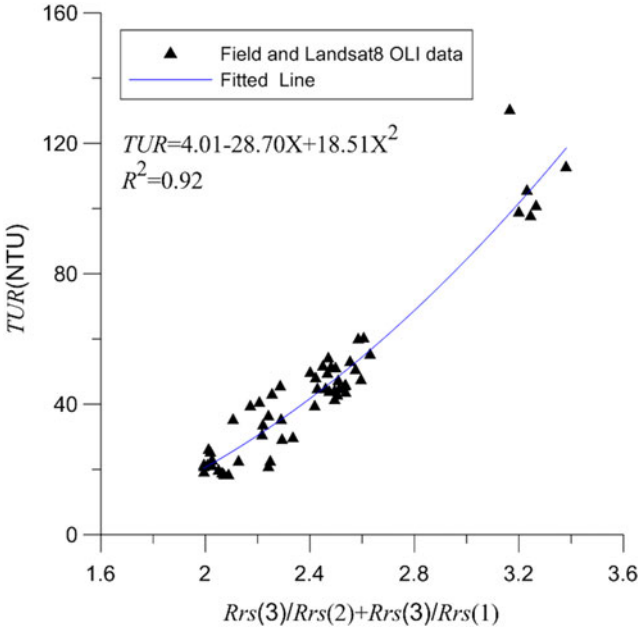

FIG. 3. *Scatter plot* and coefficient of determination between Tur and the combination factor of X consisting of Rrs at bands 1, 2, and 3 of Landsat 8 OLI. OLI, Operational Land Imager.

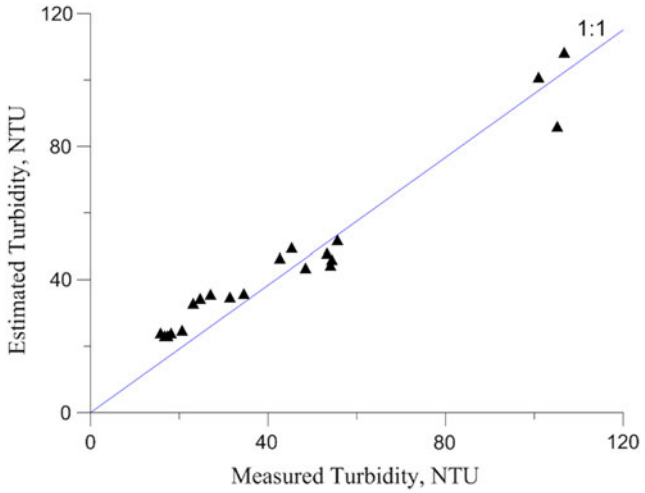

FIG. 4. Estimated turbidity from statistical model (10th) *plotted* against measured turbidity for the validation data set.

Table 4 provides model error comparisons derived during the validation phase. Tables 3 and 4 show that the tenth model outperformed the others both in establishment and validation. Taking this into account, the optimal algorithm that produced the highest determination coefficient is as follows:

$$Tur = 4.01 - 28.70X + 18.51X^2$$
$$X = R_{rs}(3)/R_{rs}(2) + R_{rs}(3)/R_{rs}(1), \quad (2)$$

where X is the combination factor of R_{rs} at band 1, band 2, and band 3, obtained from the Landsat 8 OLI. The coefficient of determination (R^2) is 0.92 for the establishment phase and 0.93 for the validation phase (Fig. 3). An F-test showed that both establishment and validation are significant below 0.01.

The measured and estimated turbidity data are distributed along a 1:1 line (Fig. 4), indicating that the statistical model can be used to estimate turbidity in the study area of the Hanjiang River. In addition, the MAE, RMSE, and MAPE of the validation data are 6.03 nephelometric turbidity units (NTU), 7.36 NTU, and 18.96%, respectively.

Results

The most stable of Landsat 8-based turbidity retrieval model from formulation set was applied to Landsat 8 OLI images taken on April 26, June 13, and November 20, 2013, and January 23, 2014, to retrieve the spatial distribution of turbidity in the Hanjiang River (Fig. 5).

The distribution frequency and descriptive statistics of derived turbidity from the four images were calculated (Table 5 and Fig. 6). The turbidity on April 26, 2013, ranged from 13.8 to 42.7 NTU with a mean of 35.6 NTU. On June 13, 2013, turbidity ranged from 35.6 to 65.5 NTU with a mean of 53.2 NTU. On November 20, 2013, turbidity ranged from 12.8 to 29.9 NTU with a mean of 25.3 NTU. On January 23, 2014, turbidity ranged from 45.1 to 150.6 NTU with a mean of 80.7 NTU. To analyze distribution of the results from different stations, turbidity acquired from OLI imagery was compared with *in situ* data (Table 1). Tables 3 and 4 and Figs. 3 and 4 show that the turbidity retrieved from the selected statistical model closely matches *in situ* data for most of the study area.

Discussion

Spatiotemporal patterns of turbidity distribution

Tables 1 and 5 and Figs. 5 and 6 indicate a region of high turbidity (about 80–150 NTU) on January 23, 2014, in the middle and downstream regions of the study area near

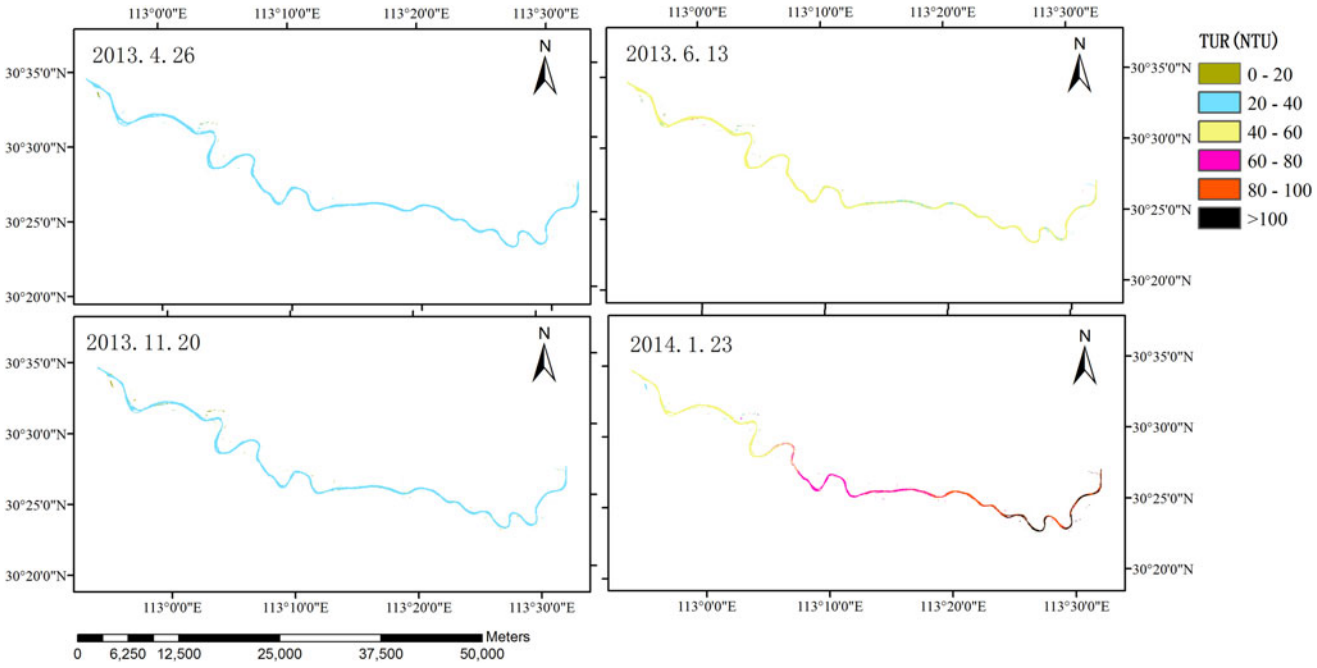

FIG. 5. Turbidity distribution estimated from first four Landsat 8 OLI images.

Table 5. Description of Landsat 8 OLI-Derived Turbidity (Nephelometric Turbidity Units) in the Study Area

Image date	*Turbidity range (NTU)*	*Mean value*	*Standard deviation*
April 26, 2013	13.8–42.7	35.6	6.50
June 13, 2013	35.6–65.5	53.2	5.38
November 20, 2013	12.8–29.9	25.3	3.54
January 23, 2014	45.1–150.6	80.7	32.15

Xiantao City. One cause of this turbidity is the intense dredging activity observed at Hanjiang River during our data collection campaigns, which resuspended sediments and increased turbidity values in the dredging region and downstream of that region. Another possible cause could be that the water level was low and flow was very weak on January 23, 2014. Table 6 provides real-time hydrological data from the Xiantao Hanjiang River Hydrological Observation station located on the south bank of the river in Xiantao City. Since the water's environmental capacity in downstream Hanjiang would decrease with a reduction in water flow and a drop of the water level (Wang *et al.*, 2004; Xie *et al.*, 2004; Li *et al.*, 2007), the river would be more sensitive to pollutants from sources (such as chemical and medical facilities) in or around Xiantao City. These could lead to high turbidity distributions in the region. Unfortunately, no water environmental parameters (such as chemical oxygen demand, dissolved oxygen, and total phosphorus) other than turbidity are available for that day.

Applicability of OLI for turbid water

The Hanjiang River plays an important role for local economical and social development as well as ecological conservation in Central China. However, like many rivers around the world, it is facing the threat of water quality degradation due to the impacts of global climate change and regional and local human activities (Wang *et al.*, 2013). In

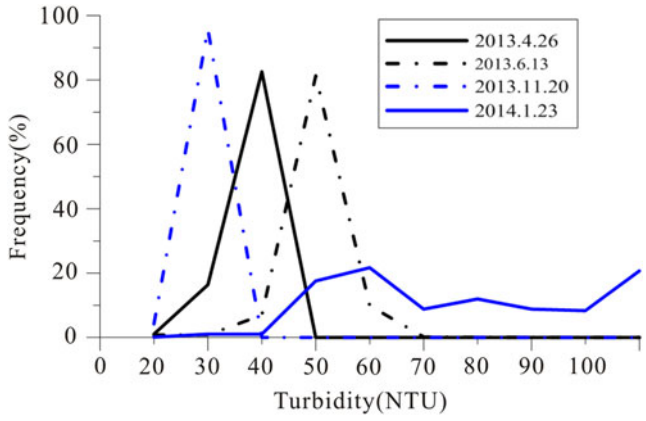

FIG. 6. Frequency distribution of turbidity in first four images from April 2013 to January 2014 estimated from Landsat 8 OLI images with the selected statistical model.

Table 6. Description of Flow and Water Level on Sampling Days

Sampling date	*Water level*	*Flow (m^3/s)*
April 26, 2013	24.19	633
June 13, 2013	25.62	858
November 20, 2013	24.07	656
January 23, 2014	23.42	455

particular, the Danjiangkou Reservoir, upstream of Hanjiang River (Fig. 1), has been used as part of the SNWDP since December 2014. Even before completion of the diversion project, spring algal blooms have occurred downstream of the Hanjiang River (Wang *et al.*, 2004, 2007). To assess whether water pollutants such as algal blooms have increased as hydrological conditions of the Hanjiang River have changed since the beginning of SNWDP water transfer, we used the retrieval model to investigate the turbidity distribution for spring of 2016 (the exact date is March 1, 2016).

Figure 7 shows a region of much higher turbidity (above 300 NTU) on March 1, 2016, near Xiantao City. News media (Changjiang Times, 2016) described an algal bloom in this area during spring of 2016. The water quality monitoring results from the Environmental Monitoring Center of Hubei Province show that the pH of the river water was weakly alkaline (8.8–9.13) and dissolved oxygen was supersaturated (13.47–14.44 mg/L), which is in accordance with the physical and chemical characteristics of the early stage of an algal bloom.

When water transfer by the SNWDP in the upstream area of the Hanjiang River began at the end of 2014, the water level decreased in mid- and downstream areas, resulting in a water level of only 23.41 m and very low flow rate (533 m^3/s) on March 1, 2016, in Xiantao City. In combination with high water temperatures, the physical conditions for an algal outbreak in Hanjiang River were met, causing high water turbidity (Wang *et al.*, 2004, 2013; Xie *et al.*, 2004). This example shows that Landsat 8 images can be used for water quality monitoring of riverine systems.

In addition, long-term spatiotemporal information of water quality parameters should be obtained by ground measurements and remote sensing observations (such as by the Landsat series) to better understand the physical and chemical characteristics of water bodies and analyze the driving factors for increased turbidity, leading to better protection of the Hanjiang River ecosystem.

Potential problems with statistical models

Normally, concurrence between satellite overpass times and field sampling is important for developing remote sensing-based turbidity retrieval models, especially for very dynamic water bodies. However, in our study, this factor was less important because there was a time delay of less than 3 h between the satellite overpass and field sampling during each field campaign, no rainfall or wind, and no significant change of water level during that period.

One Landsat 8 OLI image pixel covers a 30×30 m square or 15×15 m area, while its corresponding turbidity value is generally derived from a water sample collected at a certain location. Due to this scale gap between the image pixel and

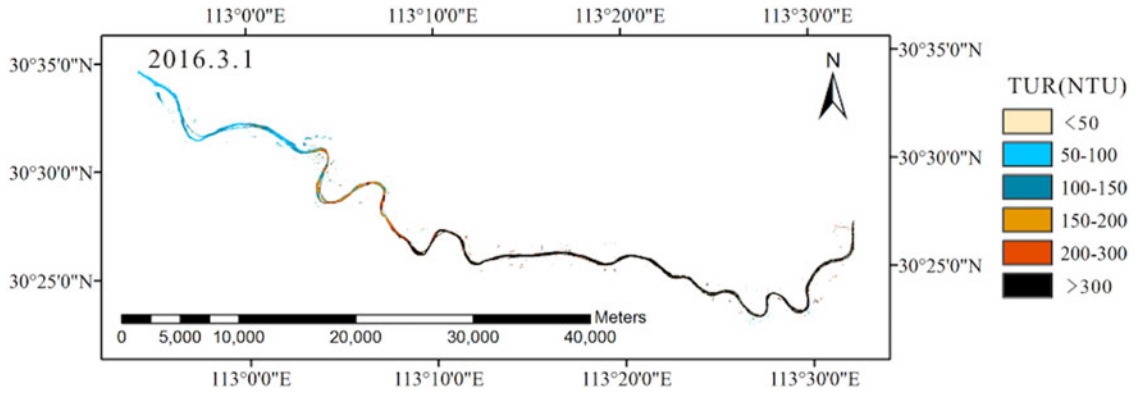

FIG. 7. Turbidity distribution estimated from the Landsat 8 OLI image on March 1, 2016.

turbidity measurement, it is generally assumed that turbidity values within a pixel are homogeneous when developing the retrieval model. However, such an assumption is not always valid for the study area because of dredging activities or localized water pollution.

Since no well-performing atmospheric algorithm for inland waters has been developed for Landsat 8 OLI images (Wu *et al.*, 2015), a simple method was employed to calculate the water-leaving reflectance of Landsat 8 OLI visible and infrared bands in this study, which might affect model development to some extent. Several methods have been applied to atmospherically correct MODIS images for estimating the water quality parameters of case II waters–atmospheric algorithms (Xie *et al.*, 2004; Li *et al.*, 2007); however, no unified atmospheric algorithm presently exists (Gordon, 1997). It would be interesting to assess the performance of these atmospheric algorithms for Landsat 8 OLI images to improve water quality retrieval in future studies. Regrettably, because the *in situ* spectral reflection of water was not measured in our field survey, and the Landsat Surface Reflectance–L8OLI/TIRS product is not available from the USGS for the study area, the validation of derived reflection could not be implemented in this study.

The statistical models developed in this study are empirical because of the absence of a strict theoretical foundation and because of different optical properties of different water bodies or even at different time periods (Wu *et al.*, 2015), which means that they cannot be applied directly to other water bodies. Another problem is the gap between the two clusters (<60 NTU and >100 NTU) of *in situ* data (Fig. 2). This may cause overfitting during model calibration. Unfortunately, no additional field surveys were conducted after February 2014 because the project had ended.

Expectations of Landsat 8 OLI

Landsat satellites have been widely used to estimate water quality parameters of inland waters (Kenier and Yan, 1998; Ko *et al.*, 2015). The latest Landsat satellite, Landsat 8 with OLI sensor, has the potential to extend more than 40 years of existing water quality estimations from Landsat satellites (Vasanthavigar *et al.*, 2011; Hong *et al.*, 2015). We expect that more robust semianalytical or statistical models will be developed for Landsat 8 images to build regional or universal models for water quality estimations of inland waters.

Conclusions

Field surveys downstream of the Hanjiang River were conducted to measure turbidity between April 2013 and January 2014. The objectives of this study were to investigate turbidity characteristics downstream of the Hanjiang River and to evaluate whether Landsat 8 OLI data could be used to monitor river water quality. The turbidity range downstream of the Hanjiang River was retrieved from Landsat 8 OLI data by employing atmospheric correction and formulating a retrieval model. Distribution trends in turbidity for the study area are consistent with field investigation results.

Results from this study show the advantages of using Landsat 8 OLI for inland riverine applications. High spatial resolution (30 m) resolves small-scale turbidity features that may otherwise go undetected, making the study of high patchiness related to suspended sediments in river systems viable.

Additional studies should be carried out to validate our findings and to obtain more accurate estimates of the spatial distribution of water quality parameters in the Hanjiang River after commencement of the SNWDP.

Acknowledgments

This work was jointly funded by the CRSRIO pen Research Program (Grant No. CKWV2016401/KY), the National Natural Science Foundation of China (Grant No. 41301098), the Science and Technology Service Network Initiative of Chinese Academy of Sciences (Grant No. KFJ-STS-ZDTP-011), and the Major Projects of Technological Innovation in Hubei Province (Grant No. 2016ACA168). The authors would like to thank the USGS for the Landsat 8 OLI data as well as the Bureau of Hydrology and Water Resources of Hubei Province for sharing hydrological data. The authors would also like to thank Feng Ling, Xiaodong Li, and LiHui Wang for their participation in the field sample collection and manuscript revision and the anonymous reviewers for their valuable comments and constructive suggestions that helped improve this article. The authors would like to thank Editage (www.editage.cn) for English language editing.

Author Disclosure Statement

No competing financial interests exist.

References

Changjiang Times. Slight Algae accured in some part of Hanjiang River. (2016). Available at: http://news.sohu.com/20160302/n439071135.shtml (in Chinese) (accessed May 30, 2016).

Davies-Colley, R.J., Smith, D.G., Ward, R.C., Bryers, G.G., McBride, G.B., Quinn, J.M., and Scarsbrook, M.R. (2011). Twenty years of Newzealand's national rivers water quality network: Benefits of careful design and consistent operation. *J. Am. Water Res. Assoc*. 47, 750.

Gerace, A.D., Schott, J.R., and Nevins, R. (2013). Increased potential to monitor water quality in the near-shore environment with Landsat's next-generation satellite. *J. Appl. Remote Sens*. 7, 1.

Ghabavati, E., Firouzabadi, P.Z., Jangi, A., and Khosravi, S. (2008). Monitoring geomorphologic changes using Landsat TM and ETM+ data in the Hendijan River delta, southwest Iran. *Int. J. Remote Sens*. 29, 945.

Gordon, H.R. (1997). Atmospheric correction of ocean color imagery in the earth observing system era. *J. Geophys. Res. Atmos*. 102, 17081.

Gordon, H.R., and Franz, B.A. (2008). Remote sensing of ocean color: Assessment of the water leaving radiance bidirectional effects on the atmospheric diffuse transmittance for SeaWiFS and MODIS inter comparisons. *Remote Sens. Environ*. 112, 2677.

Guo, Y.Q., Huang, C.C., Pang, J.L., Zha, X.C., Li, X.P., and Zhang, Y.Z. (2014). Concentration of heavy metals in the modern flood slack water deposits along the upper Hanjiang River valley, China. *CATENA* 116, 123.

Guttler, F.N., Niculescu, S., and Gohin, F. (2013). Turbidity retrieval and monitoring of Danube Delta waters using multisensor optical remote sensing data: An integrated view from the delta plain lakes to the western-northwestern Black Sea coastal zone. *Remote Sens. Environ*. 132, 86.

Hach Company. (2000). *2100P Portable Turbidimeter User Manual*. Loveland, Colorado: Hach Company.

Hong, S., Jang, H., Kim, N., and Sohn, H.-G. (2015). Water Area Extraction Using RADARSAT SAR Imagery Combined with Landsat Imagery and Terrain Information. *Sensors* 15, 6652.

Jones, J.I., Collins, A.L., Naden, P.S., and Sear, D.A. (2012). The relationship between fine sediment and macrophytes in rivers. *River Res. Appl.* 28, 1006.

Kenier, L.E., and Yan, X.H. (1998).A neural network model for estimating sea surface chlorophyll and sediments from thematic mapper imagery. *Remote Sens. Environ*. 66, 153.

Ko, B.C., Kim, H.H., and Nam, J.Y. (2015). Classification of Potential Water Bodies Using Landsat 8 OLI and a Combination of Two Boosted Random Forest Classifiers. *Sensors* 15, 13763.

Lawler, D.M., Petts, G.E., Foster, I.D.L., and Harper, S. (2006). Turbidity dynamics during spring storm events in an urban headwater river system: The Upper Tame, West Midlands, UK. *Sci. Total Environ*. 360, 109.

Le, C.F., Li,YM., Zha, Y., Sun, D.Y., Huang, C.C., and Zhang, H. (2011). Remote estimation of chlorophyll a inoptically complex waters based on optical classification. *Remote Sen. Environ*. 115, 725.

Li, C.Q., Ye, M., and Pu, H.P. (2007). Study on impact factor analysis and controlling methods of Plankton Bloom in Hanjiang River. *Environ. Sci. Survey* 26, 26. Available at: http://en.cnki.com.cn/Article_en/CJFDTOTAL-YNHK20070 2009.htm (accessed May 17, 2016).

Li, Y., Wang, Q., Wu, C., Zhao, S., Xu, X., Wang, Y.F., and Huang, C.C. (2012). Estimation of chlorophyll a concentration using NIR/red bands of MERIS and classification procedure in inland turbidwater. *IEEE Trans. Geosci. Remote Sens*. 50, 988.

Liu, J.K., and Yu, Z.T. (1992). Water-quality changes and effects on fish populations in the Hanjiang river, China, following hydroelectric DAM construction. *Regul. Rivers Res. Manage*. 7, 359.

NASA. A Closer Look at LDCM's First Scene. (2016). www.nasa.gov/mission_pageslandsat/news/first-images-feature.html

Neukermans, G., Ruddick, K.G., and Greenwood, N. (2012). Diurnal variability of turbidity and light attenuation in the southern North Sea from the SEVIRI geostationary sensor. *Remote Sens. Environ.*124, 564.

Onderka, M., and Pekárová, P. (2008). Retrieval of suspended particulate matter concentrations in the Danube River from Landsat ETM data. *Sci. Total Environ*. 397, 238.

Pahlevan, N., and Schott, J.R. (2013). Leveraging EO-1 to evaluate capability of new generation of landsat sensors for coastal/inland water studies. *IEEE J. Sel. Topics Appl. Earth Observ. Remote Sens*. 6, 360.

Simis, S.G.H., Ruiz-Verdu, A., Dominguez-Gomez, J.A., Pena-Martinez, R., Peters, S.W.M., and Gons, H.J. (2007). Influence of phytoplankton pigment composition on remote sensing of cyanobacterial biomass. *Remote Sens. Environ*. 106, 414.

Shi, K., Zhang. Y.L., Liu, X.H., Wang, M.Z., and Qin, B.Q. (2014). Remote sensing of diffuse attenuation coefficient of photosyntheticallyactive radiation in Lake Taihu using MERIS data. *Remote Sens. Environ*. 140, 365.

Shi, K., Zhang. Y.L., Zhu, G., Liu, X.H., Zhou, Y.Q., Xu, H., Qin, B.Q., Liu, G., and Li, Y.M. (2015). Long-term remote monitoring of total suspended matter concentration in Lake Taihu using 250 m MODIS-Aqua data. *Remote Sens. Environ*. 164, 43.

USGS. Landsat Missions. (2016). http://landsat.usgs.gov/index.php

Vanhellemont, Q., and Ruddick, K. (2014). Turbid wakes associated with offshore wind turbines observed with Landsat 8. *Remote Sens. Environ*. 145, 105.

Vasanthavigar, M., Srinivasamoorthy, K., Vijayaragavan, K., Gopinath, S., and Sarma, S. (2011). Groundwater potential zoning in Thirumanimuttar sub-basin Tamilnadu, India—A GIS and remote sensing approach. *Geo Spat. Inf. Sci*. 14, 17.

Vincent, R.K., Qin, X.M., Mckay, R.M., Miner, J., Czajkowski, K., Savino, J., and Bridgeman, T. (2004). Phycocyanin detection from LANDSAT TM data for mapping cyanobacterial blooms in Lake Erie. *Remote Sens. Environ*. 89, 381.

Wang, B.B., Cao, M.H., Zhu, H.D., Chen, J., Wang, L.L., Liu G.H., Gu, X.M., and Lu, X.H. (2013). Distribution of perfluorinated compounds in surface water from Hanjiang River in Wuhan, China. *Chemosphere* 93, 468.

Wang, H.P., Xia, J., Xie, P., and Dou, M. (2004). Mechanisms for hydrological factors causing algal blooms in Hanjiang river: Based on kinetics of algae grown. *Res. Environ. Yangtze Basin.* 13, 282. Available at: http://europepmc.org/abstract/cba/400955 (accessed May 17, 2016).

Wang, M.H., Tang, J.W., and Shi, W. (2007). MODIS-derived ocean color products along the China East Coastal Region. *Geophys. Res. Lett*. 34. DOI: 10.1029/2006GL028599.

Wu, G.F., Cui, L.J., Liu, L.J., Chen, F.Y., Fei, T., and Liu, Y.L. (2015). Statistical model development and estimation of suspended particulate matter concentrations with landsat 8 OLI images of Dongting Lake, China. *Int. J. Remote Sens*. 36, 343.

Xie, P., Xia, J., Dou, M., and Zhang, W.S. (2004). Research into the effects of the middle route of China's south-to-north water transfer project on water bloom in the middle-down stream of Hanjiang River and the countermeasures II:A probability analysis of the water bloom in Hanjiang River and prevention countermeasures. *J. Nat. Res*. 19, 545. Available at: http://europepmc.org/abstract/cba/462201 (accessed May 17, 2016).

Yacobi, Y.Z., Moses, W.J., Kaganovsky, S., Sulimani, B., Leavitt, B.C., and Gitelson, A.A. (2011). NIR-redreflectance-based algorithms for chlorophyll-a estimation in mesotrophic inland and coastal waters:Lake Kinneret case study. *Water Res*. 45, 2428.

Yu, Z.F., Chen, X.L., Zhou, B., Tian, L.Q., Yuan, X.H., and Feng, L. (2012). Assessment of total suspended sediment concentrations in Poyang Lake using HJ-1A/1BCCD imagery. *Chinese J. Oceanol. Limnol*. 30, 295.

Zhang, Y.B., Zhang, Y.L., Shi, K., Zha, Y., Zhou, Y.Q., and Liu, M.L. (2016b). A Landsat 8 OLI–Based, semianalytical model for estimating the total suspended matter concentration in the slightly Turbid Xin'anjiang Reservoir (China). *IEEE J. Sel. Topics Appl. Earth Observ. Remote Sens*. 9, 398.

Zhang, Y.L., Shi, K., Zhou, Y.Q., Liu, X.H., and Qin, B.Q. (2016a). Monitoring the river plume induced by heavy rainfall events in large, shallow, Lake Taihu using MODIS 250 m imagery. *Remote Sens Environ*. 173, 109.